RSC Advances

PAPER

View Article Online
View Journal | View Issue

Cite this: *RSC Adv.*, 2021, **11**, 17740

Synchronous oil/water separation and wastewater treatment on a copper-oxide-coated mesh†

Yahua Liu,[a] Peng Xu,[a] Wenna Ge,[a] Chenguang Lu,[a] Yunlai Li,[a] Shichao Niu,[b] Junqiu Zhang[b] and Shile Feng *[a]

Received 24th March 2021
Accepted 1st May 2021

DOI: 10.1039/d1ra02334a

rsc.li/rsc-advances

Despite remarkable progress in oil/water separation and wastewater treatment, the ability to carry out the two processes in a synchronous manner has remained difficult. Here, synchronous oil/water separation and wastewater treatment were proposed on mesh surfaces coated with copper-oxide particles, which possess superwetting and catalytic properties. The superwetting performance generates additional pressure to achieve the permselectivity of the designed mesh, on which the oil phase is selectively repelled while the water phase passes though easily. Moreover, the catalytic performance of the copper oxide forms reactive oxygen species to purify the water during oil/water separation process. We show that the oil/water separation and catalytic degradation efficiencies for organic pollutants can reach more than 99% by adjusting the content of copper oxide on the mesh surfaces. Such a unique design for integrating multifunctionality on single mesh surfaces strongly underpins the synchronization of oil/water separation and wastewater treatment, which will provide a new insight for separating pure water from industrial oil/water mixtures.

1. Introduction

Industrial oily wastewater and oil spill accidents bring about extensive water pollution, which have a serious impact on the environment and human health.[1] Despite various conventional methods including flotation, absorbing, filtration and centrifugation for water extraction from oily wastewater, unsatisfactory efficiency, additional energy consumption and complicated operation are always present in the process.[2–5] To address these drawbacks, functional super-wetting/anti-wetting materials including metals,[6] metal oxides and polymers have been introduced,[7–12] achieving high-efficiency and low-cost oil/water separation *via* their antipodal wettability performance for water and oil. On the one hand, oil-repellent surfaces with superhydrophilic and underwater superoleophobic properties can repel the oil completely while allowing the water phase to pass through, allowing the separation of water and oil.[13,14] On the other hand, water-repellent materials with superhydrophobic/superoleophilic properties can selectively block the water from being drawn out, allowing an efficient oil/water separation.[15–18]

Apart from oil, organic pollutants existing in oily wastewater is another major factor to affect water quality. Specifically, many of these emerging pollutants are non-biodegrade, immobile and toxic in nature, such as industry dyes, pharmaceuticals and their metabolites, disinfection by-products, *etc.*[19] Recently, extensive efforts have been directed towards addressing organic pollution in water,[20,21] among which catalytic degradation is considered as a promising approach.[22,23] For example, peroxymonosulfate (PMS), when catalytically activated by copper oxide, can generate multiple reactive oxygen species which exhibit strong degradation capacities to organic pollutions.[24]

Despite commendable progress,[25–29] one needs to assure the synchronous oil/water separation and wastewater treatment, which in practical realizations raises the issue: efficient oil/water separation and wastewater treatment in one step. To meet these requirements, in this research, an integrated multifunctional copper-oxide-coated mesh (IMCM) was designed *via* facile immersing and burning methods. By leverages the superwetting property and catalytic performance of copper oxide, the designed surface manifests synchronously high-efficiency oil/water separation and organic pollutants purification in water with peroxymonosulfate (see Video S1†). This research may promote the practical application of meshes in oil/water separation.

2. Experimental section

2.1. Surface preparation

Stainless Steel Meshes (SSM) of 500 mesh used in this work were purchased from the local market (Hebei Anping Metal Wire Manufacturing Co. Ltd., China). SSM was cut into pieces with a size 2 × 2 cm^2 and ultrasonically rinsed in acetone, anhydrous ethanol and deionized water in sequence for 10 min to remove

[a]*Key Laboratory for Precision & Non-traditional Machining Technology of Ministry of Education, Dalian University of Technology, Dalian 116024, China. E-mail: fengshile@dlut.edu.cn*

[b]*Key Laboratory of Bionic Engineering, Ministry of Education, Jilin University, Changchun 130022, China*

† Electronic supplementary information (ESI) available. See DOI: 10.1039/d1ra02334a

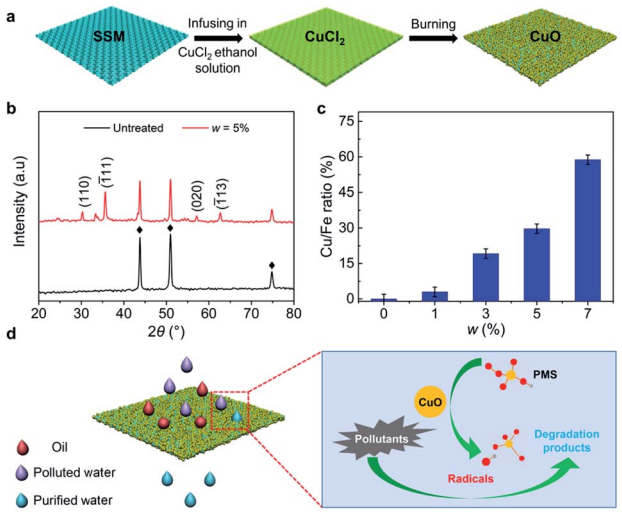

Fig. 1 Fabrication of IMCM. (a) Schematic of the fabrication process of IMCM. After simple immersing and burning, copper oxide is successfully coated on the SSM. (b) XRD analysis to confirm the chemical component on IMCM. Compared with diffraction peaks of the untreated mesh, the new peaks appeared on the IMCM with $w = 5\%$ are corresponding to the reflection of (110), ($\bar{1}11$), (020) and ($\bar{1}13$) crystal planes of CuO (JCPDS 04-009-2287). (c) The relationship between the ratio of Cu/Fe and the weight fraction (w) of $CuCl_2 \cdot 2H_2O$ solution. As the weight fraction of the solution increases, the ratio of Cu/Fe increases simultaneously. (d) Schematic of oil/water separation and wastewater treatment on IMCM. The CuO on the IMCM can activate PMS to generate radicals, which degraded the pollutants in the polluted water. The water can freely pass through the IMCM and be purified while the oil will be blocked.

undesired contamination and impurities and dried in air at ~40 °C. Then the cleaned SSM was immersed into $CuCl_2 \cdot 2H_2O$ (Tianjin Damao Chemical Reagent Factory, China) solution (solvent is ethanol) with a mass fraction (w) of 1%, 3%, 5% and 7% for 2 min. After that, the mesh surface was burned at 1000 °C for 30 s to be coated with copper oxide (Fig. 1(a)). The immersing and burning processes were repeated for three cycles.

2.2. Characterization of IMCM

The micro/nanostructures and chemical composition of IMCM surface were characterized by scanning electron microscopy (SEM, SUPRA 55 SAPPHIRE, Germany) equipped with an energy dispersive spectrometer (EDS). The contact angles of water and oil under water on the IMCM surface were measured by optical contact angle meter system (OCA25 system, Dataphysics GmbH, Germany) and determined by five individual measurements. The organics remnants in water after separation were detected by an ultraviolet-visible spectrometer (Lambda 750S, America). X-ray Diffractometer (D8 ADVANCE, Bruker Corporation) was used to observe the crystal structure of the surface.

2.3. Oil/water separation and catalytic degradation of organic pollutants

The oil/water mixtures in the experiment were composed of oil and water (with PMS of 3 mmol L^{-1}) with volume ratio 1 : 1. The water and oil were dyed to blue and red color with methylene blue (MB, 5 mg L^{-1}) and Sudan III (5 mg L^{-1}), respectively. Here, MB and Rhodamine B were chosen as organic pollutants to evaluate the catalytic degradation efficiency of IMCM. The device (Fig. S1†) for oil/water separation was designed by fixing the IMCM surface between two glass tubes, which can synchronously achieve oil/water separation and catalytic degradation of organic pollutants. The oil/water mixture was poured into the upper glass tube and the whole separation proceeded by gravity, which was recorded by a digital single lens reflex camera (Canon, EOS 80D, Japan). The separation efficiency (E_s) can be defined as $E_s = m_{aw}/m_{ow}$. Here m_{aw} and m_{ow} are the mass of water after separation and the mass of water in the original oil/water mixtures, respectively. The flux (F) of the mesh is depicted as $F = V/St$. Here V, S, and t represent the volume of water, the effective area of the mesh and the whole separating time, respectively. The catalytic degradation efficiency (E_c) is calculated as $E_c = (C_0 - C)/C_0$. Here C_0 and C are the concentration of organic pollutants before and after catalytic degradation.

3. Results and discussion

3.1. Fabrication of IMCM

Materials with superwetting and catalytic performances are the foundation for synchronous oil/water separation and organic pollutants purification in one step. Fortunately, copper oxide is a paragon that synergizes these two properties. In this regard, we fabricated an integrated multifunctional copper-oxide-coated mesh (IMCM) *via* immersing SSM into $CuCl_2 \cdot 2H_2O$ solution for 2 min and burning at 1000 °C for 30 s (Fig. 1(a)). The mass fraction (w) of $CuCl_2 \cdot 2H_2O$ solution are 0%, 1%, 3%, 5%, 7%, respectively. Note that IMCM with $w = 0\%$ means that the SSM is only cleaned but without any further treatment for comparison. The chemical reactions in the preparation are as follows:

$$Cu^{2+} + 2OH^- \triangleq Cu(OH)_2 \quad (1)$$

$$Cu(OH)_2 \triangleq CuO + H_2O \quad (2)$$

To confirm the chemical components of the fabricated surface, we performed X-ray diffraction (XRD) analyses on IMCM with w of 5% (Fig. 1(b)). For untreated SSM, the peaks marked with asterisk can be indexed to austenite (FeCr0·29Ni0·16C0.06), which is the major component of the SSM. For IMCM, the new characteristic diffraction peaks corresponding to the reflection of (110), ($\bar{1}11$), (020) and ($\bar{1}13$) crystal planes of monoclinic CuO phase (JCPDS 04-009-2287) are appeared, which indicates that CuO is successfully coated on designed surface. In addition, the EDS measurement shows that Cu and O elements are existed on IMCM and the ratio of Cu/Fe element can be controlled from 3% to 58% by mediating the value of w (Fig. 1(c) and Fig. S2†). The morphologies of IMCM with different w were shown in Fig. S3.† For cleaned mesh without further treatment ($w = 0\%$), the surface is smooth (Fig. S3(a)†). With the increase of w, nanoparticles are formed on the surface and the size of particles increases gradually with

formed overlapping and stacking structures (Fig. S3(b–e)).† Further SEM images show that the nanoparticles also distribute uniformly on the cross section of IMCM (Fig. S4†). Combination of the results shown in EDS and SEM measurements, we obtain that the nanoparticles are CuO, which successful grow on IMCM.

3.2. Superwetting and catalytic performance of IMCM

To examine the superwetting performance of IMCM, we measured its water contact angle (θ_w) and underwater oil contact angle (θ_{oil}) on the surfaces which were treated with w of 0%, 1%, 3%, 5%, 7%, respectively. Here the oil is dichloroethane. For $w = 0\%$, the mesh manifests a θ_w of 78° ± 2.0° and underwater θ_{oil} of 124° ± 1.8° (Fig. S5(a and b)†). For w of 1%, 3%, 5%, 7%, superhydrophilicity and underwater superoleophobicity are achieved with an average θ_w and θ_{oil} of ~0° and 157°, respectively (Fig. 2(a) and S5(c), S5(d)).† We also tested the dynamic wettability of the mesh treated with various value of w (Fig. S6†). It is clear to see that for $w < 5\%$, $\theta_{SA} > 20°$ and for $w \geq 5\%$, $\theta_{SA} < 10°$. Therefore, we obtain that IMCM treated with $w \geq 5\%$ manifests superoleophobicity and low-adhesion underwater. The superhydrophilicity and underwater superoleophobicity also applied to other types of oil, as exemplified in Fig. S7.† We demonstrate that the excellent superwetting performance of IMCM is mainly determined by the coated hydrophilic chemical component of CuO and could be enhanced by surface micro/nano structures, which guarantees the water to pass through the mesh while the oil to be repelled (Fig. 1(d)).

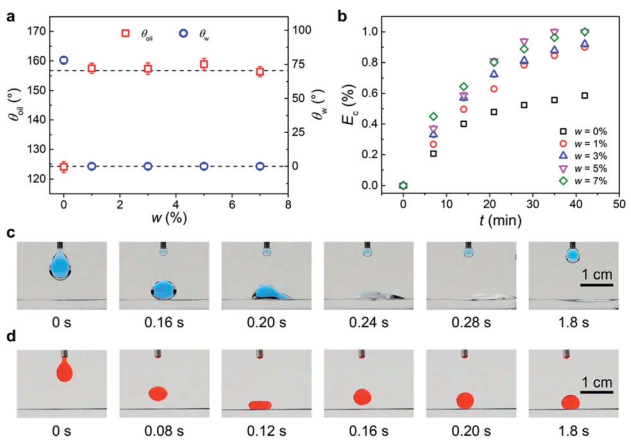

Fig. 2 Superwetting and catalytic performance of IMCM surfaces. (a) The influence of w on θ_w and underwater θ_{oil}. For $w = 0\%$ (untreated mesh), θ_w was ~78° while θ_{oil} was ~124°. After treatment, the averages of the θ_w and θ_{oil} on the IMCM surfaces were maintained at ~0° and ~157°, respectively. (b) Changing of E_c over time on the surface with different w. The influence of w on E_c over time. When $w < 5\%$, the performance of the catalytic degradation was gradually increasing with the growth of the w. When $w > 5\%$, however, redundant CuO may scavenge some generated radicals and then lead to the decrease of catalytic efficiency. (c) Dynamic process of water droplet on the IMCM surface. Under oil (liquid paraffin), the water droplet contained MB and PMS can spread and pass through the IMCM in 1.8 s. During this process, the CuO on the IMCM can activate PMS to degrade the MB to make the droplet transparent. (d) Dynamic process of oil droplet (dichloroethane) on IMCM. Under water, the oil droplet can rapidly rebound after impacting the IMCM for its low adhesion with the substrate.

To validate the catalytic performance of the surface, the IMCM surface was immersed in a mixed solution containing 5 mg L^{-1} MB^{-1} and 3 mmol L^{-1} PMS, with deionized water as the solvent. The catalytic degradation efficiency (E_c) is calculated as $E_c = (C_0 - C)/C_0$, where C_0 and C are the concentration of MB before and after catalytic degradation, respectively. As shown in Fig. 2(b), E_c increases gradually and then maintains unchanged over time. Note that, the IMCM surface with $w = 5\%$ achieves the optimal catalytic degradation performance, which degrades almost all the organic pollutions in water in the shortest time. As has been studied in previous research, the lower content of CuO limits the surface catalytic efficiency for $w < 5\%$. While for $w > 5\%$, redundant CuO may scavenge some generated radicals and thus reduces the catalytic efficiency.[30,31] Therefore, IMCM surface ($w = 5\%$) with the optimal catalytic efficiency is selected for further exploration.

To verify the superwetting and catalytic performance, we visualize the dynamic process of droplets on IMCM with $w = 5\%$. Here the water droplet including PMS and oil droplet (dichloroethane) are dyed to blue and red color by MB and Sudan III, which are chosen as organic pollutants. During this test, the IMCM was pre-wetted by water because it is not superhydrophilic without pre-wetting under oil (liquid paraffin) environment (Fig. S8†). For water droplet in oil medium, as shown in Fig. 2(c), the water spreads and passes through IMCM rapidly in less than 1.8 s. Strikingly, the water droplet becomes transparent gradually due to the degradation of MB by multiple reactive oxygen species which is generated in catalytically activating process. This result sharply contrasts with the observation of the dynamics process of oil droplet in water medium (Fig. 2(d)), where the oil droplet manifests a ball shape and very low interface adhesion for a thin water film generated between the oil and IMCM surface (Fig. S5(d)).† The dynamic behaviors of water and oil droplets indicate that IMCM possesses excellent superhydrophilicity, underwater superoleophobicity and catalytic degradation performance of organic pollutants, which is consistent with that shown in Fig. 2(a) and (b).

3.3. Oil/water separation performance

In the oil/water separation process, we pour the oil/water mixture with a volume ratio of 1 : 1 into the upper glass tube of a separating unit which is composed by fixing the IMCM between two glass tubes (Fig. S1†). As shown in Fig. 3(a), the water passes through the IMCM easily, while the oil is completely blocked (see Video S2†). Moreover, the maximum height of blocked n-hexane column (h_{max}) can reach up to ~31 cm (Fig. 3(b)), corresponding to a maximum hydrostatic pressure of ~2 kPa. This critical pressure is called breakthrough pressure (ΔP), which is defined as the maximum pressure applied on the surface before the liquid permeates into the surface pore structure.

The breakthrough pressure is determined by both the surface wetting properties and structures. For pores with

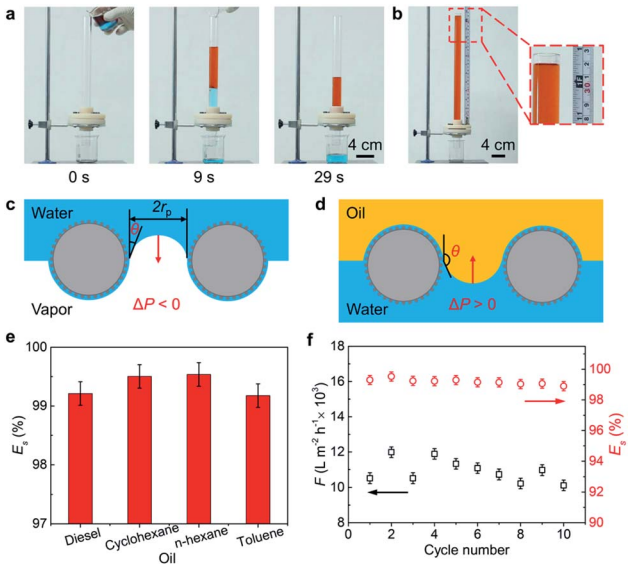

Fig. 3 Oil/water separation performance of IMCM. (a) Sequential images showing the oil/water separation process, during which the water passes through the IMCM easily, while the oil is completely blocked. (b) The maximum height of blocked *n*-hexane column on the IMCM surface. (c) The schematic showing the interaction mechanism between water and the IMCM surface. (d) The schematic showing the interaction mechanism between oil and IMCM surface. (e) The oil/water separation efficiency of mixtures composed of oil (diesel, cyclohexane, *n*-hexane, toluene) and water. (f) The value of E_s and F in 10 cycles. It is clear to see that both E_s and F change little in 10 cycles.

a cylindrical geometry, ΔP can be depicted as: $\Delta P = -2\gamma \cos\theta/r$, with γ, r and θ represent the surface tension of the liquid, the radius of the pores, and the intrinsic contact angle of the liquid on a flat surface, respectively.[32] In the absence of external forces, liquid can pass through pore structures with $\Delta P < 0$, while be blocked with $\Delta P > 0$.[33] In our experiment, superhydrophilic surface with θ_w of ~0° is formed on designed IMCM surface, which causes a negative ΔP to promote water to pass through the surface spontaneously (Fig. 3(c)). While due to underwater superoleophobicity with average θ_{oil} of ~157°, the ΔP of different kinds of oils is always positive (Table S1†) that forms a blocking effect for oil (Fig. 3(d)). The water anti-blocking and oil blocking effect provide a guarantee for the efficient oil/water separation.

We further explored the separation efficiency (E_s) in oil/water separating process on IMCM surface. It is clear that the E_s always exceeds 99% for different kinds of oil/water mixtures, as shown in Fig. 3(e). Not only separation efficiency, but also flux (F) of water is an important index for evaluating oil/water separation ability. On the fabricated surface, the F of water can reach up to 10 000 L m^{-2} h^{-1}. Note that, E_s and F are both little changed in 10 cycles on the IMCM surface, indicating an efficient and stable oil/water separation performance (Fig. 3(f)). This result is attributed to the outstanding self-cleaning ability of IMCM, *e.g.*, the oil attached to the surface is easily removed due to the repelling effect of a thin water film generated between oil and IMCM surface (Fig. S5(d) and S9†).

3.4. Synchronous oil/water separation and wastewater treatment

Achieving synchronous oil/water separation and wastewater treatment is a great challenge for the time delay of catalytic performance. To address this drawback, a porous filter paper was added on the IMCM surface to slow down the passing velocity of oil/water mixtures. Here, the water (with PMS of 3 mmol L^{-1}) contains 5 mg L^{-1} MB^{-1} as organic pollutants to evaluate the catalytic degradation efficiency of the IMCM while the oil is *n*-hexane. For IMCM surfaces treated with series of w, the water and oil can be separated completely. Further observation reveals that the water separated by IMCM with $w = 0\%$ always stays blue with a slightly lighter in 35 min, due to the degradation ability of PMS (Fig. S10†). In contrast, the water separated by IMCM with $w = 5\%$ fades gradually and finally becomes transparent (Fig. 4(a)), which is attributed to the gradual catalytic degradation of MB in water, as evidenced by the peak height of UV-vis absorbance spectrum of MB (Fig. 4(b)). This result indicates that IMCM surface with $w = 5\%$ exhibits excellent synchronous oil/water separation and wastewater treatment performance. We also measured the catalytic degradation of IMCM to other organic pollutants, *e.g.*, rhodamine B. It is clear that IMCM with $w = 5\%$ manifests an excellent E_c of almost 100% in 12 min, while IMCM with $w = 0\%$ manifests an

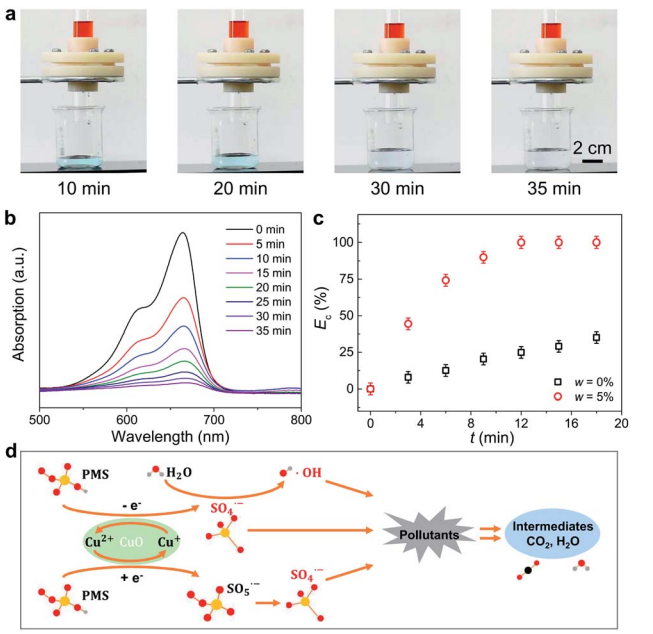

Fig. 4 Catalytic degradation performance of IMCM. (a) Sequential images showing the oil/water separation and catalytic degradation process. The MB in the water can be gradually degraded when the water passed passes through the IMCM surface, and finally, the water collected was is totally transparent. The oil in this test is *n*-hexane. (b) The detected UV-vis absorbance spectrum of MB during the catalytic degradation. The height of the peak gradually decreased decreases over time. (c) The catalytic degradation performance of the IMCM to RhB. RhB was is only degraded 25% on IMCM surface with $w = 0\%$ after 12 minutes. While the E_c was is close to 100% on the IMCM with $w = 5\%$. (d) The schematic showing the catalytic degradation mechanism.

E_c of 25% (Fig. 4(c)). This further indicates that the catalytic degradation performance of IMCM with $w = 5\%$ is robust for various kinds of organic pollutants.

The catalytic degradation performance of IMCM differed depending on whether or not CuO is present. In our experiment, CuO acts as a catalyst, which can activate PMS to generate multiple reactive oxygen species for high-efficiency degradation of organic pollutions (Fig. 4(d)). The reaction equations are depicted as:

$$\equiv Cu^{2+} + HSO_5^- \rightarrow \equiv Cu^+ + SO_5^{\bullet -} + H^+ \quad (3)$$

$$2SO_5^{\bullet -} \rightarrow 2SO_4^{\bullet -} + O_2 \quad (4)$$

$$\equiv Cu^+ + HSO_5^- \rightarrow Cu^{2+} + SO_4^{\bullet -} + OH^- \quad (5)$$

$$SO_4^{\bullet -} + H_2O \rightarrow {}^{\bullet}OH + SO_4^{2-} + H^+ \quad (6)$$

$$SO_4^{\bullet -} + {}^{\bullet}OH + \text{pollutants} \rightarrow \text{intermediates} + CO_2 + H_2O + SO_4^{2-} \quad (7)$$

First, the Cu^{2+} is reduced to Cu^+ in the presence of PMS and the PMS is activated to $SO_5^{\bullet -}$ and $SO_4^{\bullet -}$ (eqn (3) and (4)).[34,35] Subsequently, the Cu^+ will react with the PMS to produce $SO_4^{\bullet -}$ (eqn (5)).[21] Besides, some $SO_4^{\bullet -}$ radicals will react with H_2O to generate ${}^{\bullet}OH$ (eqn (6)).[36] In these processes, the Cu^{2+} and Cu^+ act as catalyst *via* converting to each other with electron transfer. Finally, the generated reactive oxygen species ($SO_4^{\bullet -}$, ${}^{\bullet}OH$) can degrade the organic pollutions into intermediates, CO_2 and H_2O (eqn (7)) and achieve wastewater treatment.[37]

4. Conclusion

In this research, we report a unique strategy for synchronous oil/water separation and wastewater treatment in one step on integrated multifunctional copper-oxide-coated mesh (IMCM) surfaces. The fabricated IMCM surface exhibits oil/water separation and catalytic degradation efficiencies of more than 99%. We show that such excellent capacities are underpinned by the superwetting and catalytic properties of copper oxide: the superhydrophilic ability generates additional pressure to facilitate the penetration of water while blocking the oil, endowing an efficient oil/water separation; in addition, the copper oxide forms reactive oxygen species to degrade organic pollution during water penetration process. This synchronization strategy will enhance the pure water separation efficiency from industrial oily sewage.

Author contributions

The manuscript was written through contributions of all authors. All authors have given approval to the final version of the manuscript.

Conflicts of interest

The authors declare no competing financial interest.

Acknowledgements

We are grateful for the support from National Natural Science Foundation of China (52075071, 51605073, 52005075), the Fundamental Research Funds for the Central Universities (DUT18RC(3)048, DUT19RC(3)055), Liao Ning Revitalization Talents Program (XLYC1807092) and Opening Project of the Key Laboratory of Bionic Engineering (Ministry of Education), Jilin University (KF20200002). Y. L. and S. F. acknowledge support from the Star Ocean Outstanding Talents Program.

Notes and references

1 B. Jiang, H. Zhang, L. Zhang, Y. Sun, L. Xu, Z. Sun, W. Gu, Z. Chen and H. Yang, *Ind. Eng. Chem. Res.*, 2017, **56**, 11817–11826.
2 O. Abdelwahab, N. K. Amin and E. S. Z. El-Ashtoukhy, *J. Hazard. Mater.*, 2009, **163**, 711–716.
3 X. Bai, Z. Zhao, H. Yang and J. Li, *Sep. Purif. Technol.*, 2019, **221**, 294–302.
4 G. Zhang, Y. Li, A. Gao, Q. Zhang, J. Cui, S. Zhao, X. Zhan and Y. Yan, *Chem. Eng. J.*, 2019, **369**, 576–587.
5 M. Ge, C. Cao, J. Huang, X. Zhang, Y. Tang, X. Zhou, K. Zhang, Z. Chen and Y. Lai, *Nanoscale Horiz.*, 2018, **3**, 235–260.
6 S. Feng, Y. Xing, S. Deng, W. Shang, D. Li, M. Zhang, Y. Hou and Y. Zheng, *Adv. Mater. Interfaces*, 2018, **5**, 1701193.
7 I. Sadeghi, N. Govinna, P. Cebe and A. Asatekin, *ACS Appl. Polym. Mater.*, 2019, **1**, 765–776.
8 N. Govinna, I. Sadeghi, A. Asatekin and P. Cebe, *J. Polym. Sci., Part B: Polym. Phys.*, 2019, **57**, 312–322.
9 L. Tang, Z. Zeng, G. Wang, L. Shen, L. Zhu, Y. Zhang and Q. Xue, *ACS Appl. Mater. Interfaces*, 2019, **11**, 18865–18875.
10 M. Wang, Z. Xu, Y. Guo, Y. Hou, P. Li and Q. J. Niu, *J. Membr. Sci.*, 2020, **611**, 118409.
11 L. Feng, Z. Zhang, Z. Mai, Y. Ma, B. Liu, L. Jiang and D. Zhu, *Angew. Chem., Int. Ed.*, 2004, **43**, 2012–2014.
12 L. Qiu, Y. Sun and Z. Guo, *J. Mater. Chem. A*, 2020, **8**, 16831–16853.
13 J. Li, L. Yan, H. Li, W. Li, F. Zha and Z. Lei, *J. Mater. Chem. A*, 2015, **3**, 14696–14702.
14 M. Liu, S. Wang and L. Jiang, *Nat. Rev. Mater.*, 2017, **2**(7), 17036.
15 Y. Si, Q. Fu, X. Wang, J. Zhu, J. Yu, G. Sun and B. Ding, *ACS Nano*, 2015, **9**, 3791–3799.
16 J. Ge, L. A. Shi, Y. C. Wang, H. Y. Zhao, H. Bin Yao, Y. B. Zhu, Y. Zhang, H. W. Zhu, H. A. Wu and S. H. Yu, *Nat. Nanotechnol.*, 2017, **12**, 434–440.
17 W. Zhang, Z. Shi, F. Zhang, X. Liu, J. Jin and L. Jiang, *Adv. Mater.*, 2013, **25**, 2071–2076.
18 J. Yuan, X. Liu, O. Akbulut, J. Hu, S. L. Suib, J. Kong and F. Stellacci, *Nat. Nanotechnol.*, 2008, **3**, 332–336.
19 W. Da Oh, Z. Dong and T. T. Lim, *Appl. Catal., B*, 2016, **194**, 169–201.
20 N. H. Tran, T. Urase, H. H. Ngo, J. Hu and S. L. Ong, *Bioresour. Technol.*, 2013, **146**, 721–731.

21 M. Bilal, M. Adeel, T. Rasheed and H. M. N. Iqbal, *J. Mater. Res. Technol.*, 2019, **8**, 2359–2371.
22 S. Rojas and P. Horcajada, *Chem. Rev.*, 2020, **120**, 8378–8415.
23 H. Meng, C. Nie, W. Li, X. Duan, B. Lai, Z. Ao, S. Wang and T. An, *J. Hazard. Mater.*, 2020, **399**, 123043.
24 F. Mushtaq, X. Chen, H. Torlakcik, B. J. Nelson and S. Pané, *Nano Res.*, 2020, **13**, 2183–2191.
25 J. Wang and S. Wang, *Chem. Eng. J.*, 2018, **334**, 1502–1517.
26 Z. Lei, J. Feng, Y. Yang, J. Shen, W. Zhang and C. Wang, *J. Hazard. Mater.*, 2020, **382**, 121057.
27 Y. Zhu, D. Wang, L. Jiang and J. Jin, *NPG Asia Mater.*, 2014, **6**, e101.
28 J. Y. Huang, S. H. Li, M. Z. Ge, L. N. Wang, T. L. Xing, G. Q. Chen, X. F. Liu, S. S. Al-Deyab, K. Q. Zhang, T. Chen and Y. K. Lai, *J. Mater. Chem. A*, 2015, **3**, 2825–2832.
29 J. Song, S. Huang, Y. Lu, X. Bu, J. E. Mates, A. Ghosh, R. Ganguly, C. J. Carmalt, I. P. Parkin, W. Xu and C. M. Megaridis, *ACS Appl. Mater. Interfaces*, 2014, **6**, 19858–19865.
30 J. Yan, J. Li, J. Peng, H. Zhang, Y. Zhang and B. Lai, *Chem. Eng. J.*, 2019, **359**, 1097–1110.
31 B. C. Gilbert and J. K. Stell, *J. Chem. Soc., Faraday Trans.*, 1990, **86**, 3261–3266.
32 M. A. Gondal, M. S. Sadullah, M. A. Dastageer, G. H. McKinley, D. Panchanathan and K. K. Varanasi, *ACS Appl. Mater. Interfaces*, 2014, **6**, 13422–13429.
33 C. Chen, D. Weng, A. Mahmood, S. Chen and J. Wang, *ACS Appl. Mater. Interfaces*, 2019, **11**, 11006–11027.
34 M. Xu, J. Li, Y. Yan, X. Zhao, J. Yan, Y. Zhang, B. Lai, X. Chen and L. Song, *Chem. Eng. J.*, 2019, **369**, 403–413.
35 Z. Yang, D. Dai, Y. Yao, L. Chen, Q. Liu and L. Luo, *Chem. Eng. J.*, 2017, **322**, 546–555.
36 Z. Li, D. Liu, Y. Zhao, S. Li, X. Wei, F. Meng, W. Huang and Z. Lei, *Chemosphere*, 2019, **233**, 549–558.
37 J. Zou, J. Ma, L. Chen, X. Li, Y. Guan, P. Xie and C. Pan, *Environ. Sci. Technol.*, 2013, **47**, 11685–11691.